Fingerprints of random flows?

Michael Wilkinson,[1] Vlad Bezuglyy,[1] and Bernhard Mehlig[2]
[1]*Department of Mathematics and Statistics, The Open University, Walton Hall, Milton Keynes MK7 6AA, England*
[2]*Department of Physics, Göteborg University, 41296 Gothenburg, Sweden*

(Received 18 September 2008; accepted 18 March 2009; published online 24 April 2009)

We consider the patterns formed by small rodlike objects advected by a random flow in two dimensions. An exact solution indicates that their direction field is nonsingular. However, we find from simulations that the direction field of the rods does appear to exhibit singularities. First, "scar lines" emerge where the rods abruptly change direction by π. Later, these scar lines become so narrow that they "heal over" and disappear, but their ends remain as point singularities, which are of the same type as those seen in fingerprints. We give a theoretical explanation for these observations. © *2009 American Institute of Physics*. [DOI: 10.1063/1.3118502]

I. INTRODUCTION

We consider the motion of small rodlike particles suspended in a moving fluid. The suspended particles align with their neighbors in a manner determined by the strain rate of the flow. In a turbulent or randomly moving fluid, the direction vector field of the rods forms complex textures, illustrated by Fig. 1. We concentrate on two-dimensional textures because it is hard to observe the direction field in three dimensions. Also, we confine attention to the case of incompressible flow, which is easiest to analyze and which is easily realized experimentally (by using a suspension of rodlike particles in a film of water floating upon a denser fluid which is randomly stirred). The results are of quite general interest because any asymmetric particles will have a preferred direction determined by the history of the strain tensor of the field along the trajectory of the particle.

Suspensions of small anisotropic particles called rheoscopic fluids are often used for flow visualization.[1–3] This uses the principle that the intensity of scattering of light from a localized source will depend on the orientation of the suspended particles. The information in this visualization can be enhanced by using light sources with different colors.[4] In this paper we show how the colors might be used to reveal information about the topology of the textures formed by the rheoscopic fluid. In Fig. 2 we demonstrate the potential of this approach for rodlike particles. For illustrative purposes, we assume that the intensity of scattering from a rod at angle θ from a source at angle ϕ (relative to a line perpendicular to the rod) is proportional to $\cos^2(\theta-\phi)$ (this approximation can be justified when the rods are short compared to the wavelength of the light). Accordingly, in Fig. 2 we redisplay the textures in Fig. 1 by plotting a color C which is an admixture of the primary colors red, green, and blue, denoted (R,G,B),

$$C = R\cos^2(\theta) + G\cos^2(\theta - 2\pi/3) + B\cos^2(\theta - 4\pi/3). \tag{1}$$

(In Fig. 2 the angle θ of the rods is measured relative to the horizontal, with θ increasing in the anticlockwise direction.) The physics of scattering or reflection from the rodlike particles is complex, but this illustration is indicative of what can be seen with different colored light sources.

The rod direction field is a nonoriented vector field in a two-dimensional space (by nonoriented, we mean that rod directions differing by π are equivalent). In such a field we might expect to see point singularities of the direction field of the type illustrated in Fig. 3, which are also present in fingerprint patterns[5] (where the patterns formed by ridges are another example of a nonoriented vector field in two dimensions). The actual textures that we observe in simulations do indeed have structures which resemble the core and delta singularities of fingerprints, as illustrated by the examples in Fig. 1. We shall argue that the principles underlying the structures visible in this picture are quite subtle, and that it is, in fact, surprising to see such singularities. We remark that the singularities are characterized by a topological invariant, termed the Poincaré index, which is illustrated in Fig. 4, and topological arguments will be central to the discussion. Singularities with a nonzero Poincaré index could be detected using the visualization technique illustrated in Fig. 2, by examining the colors along a closed path. If the colors cycle through all three primaries as the path is traversed, this path must contain a singularity of the rod directions. The sign of the Poincaré index is determined by the order in which the primary colors cycle ($R\to G\to B$ or $R\to B\to G$).

In Sec. II below we give a simple derivation of the equation of motion for the rods and present its general solution. Our equation of motion is a limiting case of that given by Jeffery[6] for the motion of an ellipsoid of revolution in a viscous fluid at low Reynolds number. He also obtained the solution for a simple shear flow, showing that ellipsoids with a finite aspect ratio undergo a tumbling motion (although the rods which are considered here simply tilt into the shear plane). In this paper we use a general solution of Jeffery's nonlinear equation of motion in terms of a companion linear equation. The same solution is given by Szeri,[7] who refers to earlier works[8,9] which contain related ideas, but not the full solution. In Sec. II we discuss a form of the general solution which is specific to the limiting case of rodlike particles, but

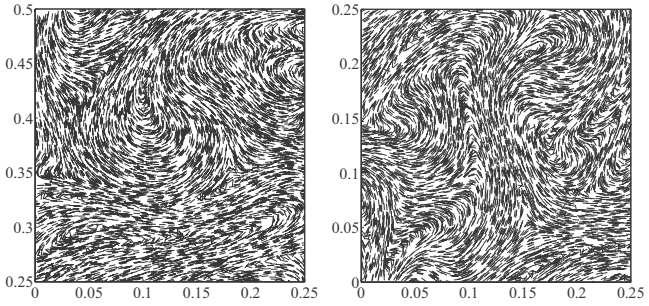

FIG. 1. Simulations of the orientations of rods advected by a random flow in two dimensions. These appear to show singularities which are analogous to those occurring in fingerprint patterns, illustrated in Fig. 3. The simulations describe a dilute suspension of very small rods: here their sizes are exaggerated to make the textures visible. Details of the simulations are specified in the Appendix.

we remark that the same approach is readily extended to general axisymmetric bodies and to three-dimensional flows.[7]

Several authors have discussed the dynamics of rodlike objects at low Reynolds number in flows with nonuniform shear. Szeri[7] considered the tumbling motion of ellipsoidal particles in recirculating flows, making some use of the companion linear equation, but relying mainly upon applying ideas from dynamical system theory applied to the nonlinear equation obtained by Jeffery.[6] A later paper by Szeri and Leal[10] made more extensive use of the companion linear equation. Several other authors have considered chaotic aspects of the motion of ellipsoids in more complex flows.[11–14]

Section III discusses the extent to which the solution we describe in Sec. II can exhibit singularities. We start by presenting an argument showing that the direction field cannot have any singularities. This implies that the Poincaré index for any curve is zero and is hard to reconcile with the appearance of Figs. 1 and 2. Throughout most of the plane the direction field of the rods is asymptotic to the eigenvector field of the monodromy matrix of the fluid flow. However, the eigenvector field can have a nonzero Poincaré index implying that the asymptotic correspondence between these vector fields breaks down somewhere. We show that it fails along certain lines, which we term *scar lines*, where the direction vector of the rods abruptly changes by π. The scar line emerges and sharpens as the two vector fields asymptotically approach each other. As the scar line (illustrated in Fig. 5) sharpens, there will be fewer rods which lie in the region where the direction differs from the asymptotic value. The result is that the scar line disappears (see Fig. 6). At the ends of the scar line there remains a point singularity of the type illustrated in Fig. 3.

In Sec. IV we consider the behavior of our solution of the equation of motion discussed in Sec. II in the long-time limit. The solution appears to be incompatible with a statistically stationary limit, but this is shown not to be the case. We also show that the probability distribution of the gradient of the angle has an approximately log-normal distribution. This is consistent with the existence of apparent singularities in the rod textures, where the angle of the rods changes very abruptly. Section V summarizes the results and discusses how the patterns observed at long times can be understood. The numerical simulations are described in the Appendix.

We stress that in this paper the rodlike particles in the fluid are assumed to be so small and so dilute that they do not influence the fluid flow and are unlikely to come into contact with each other (the sizes of the rods in Fig. 1 have been grossly exaggerated to make the pattern visible). This assumption is valid for most applications of rheoscopic suspensions, which reflect light effectively even at very small volume fractions. A nematic liquid crystal consists of rodlike molecules (either a pure substance or diluted with a solvent), and it is natural to consider whether our results have any relevance to such systems. There appears to be little connection between the dilute limit which we consider, where the rod orientation satisfies a differential equation, and the physics of liquid crystals, where the orientation vector field minimizes an energy functional, known as the *Oseen–Frank functional*.[15] In addition to static studies of their textures, there is also an extensive literature on the dynamics of liquid crystals: see, for example, Ref. 16 and references therein.

II. EQUATION OF MOTION AND ITS SOLUTION

A. Derivation of the equation of motion

While the equation of motion which we consider is a limiting case of that derived by Jeffery,[6] the general calculation is quite lengthy and insight is gained from a simple derivation. Strictly speaking, in the calculation below we consider the motion of *dumbells*, that is, pairs of particles (which are dragged by the fluid) connected by a rigid rod

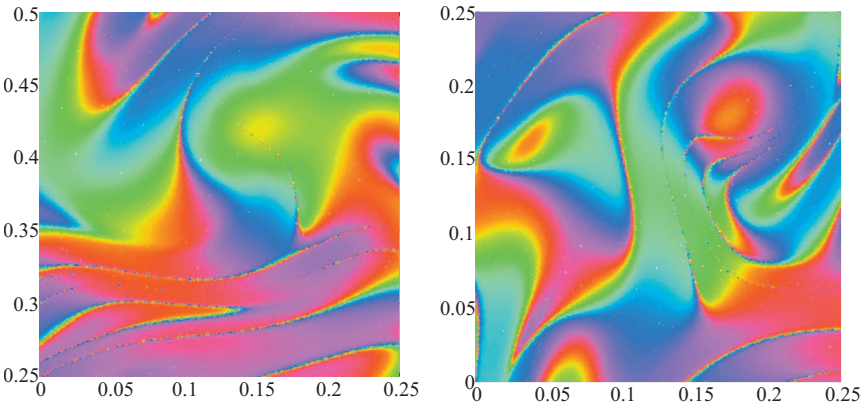

FIG. 2. (Color) The rod textures shown in Fig. 1 color coded using Eq. (1), to illustrate how the textures can be visualized using colored light sources.

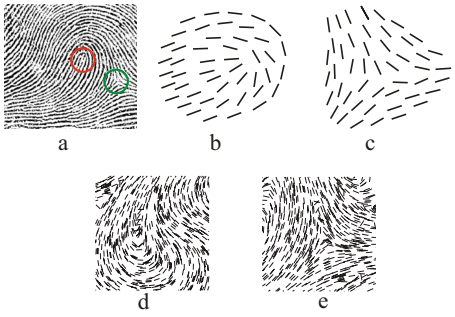

FIG. 3. (Color online) The textures illustrated in Fig. 1 have similarities with fingerprints patterns, such as (a) (taken from Ref. 5). Such patterns contain two elementary point singularities of nonoriented vector fields in two dimensions: in fingerprint patterns these are known as the *core* (b) and the *delta* (c), marked by circles (online, in red and green, respectively) in (a). Examples of these singularities as they appear in rod textures are shown in (d) and (e), respectively.

(which is not influenced by the flow). However, the equation of motion we obtain is independent of the length a of the rod in the limit as $a \to 0$, and by imagining a rod as being formed by overlaying dumbells of different lengths, we surmise that our equation describes a short symmetric rod with a general distribution of its viscous drag along its length. The rods are advected by a velocity field $\boldsymbol{v}(\boldsymbol{r},t)$, which is characterized by a correlation time τ, correlation length ξ, and typical magnitude v_0. In a multiscale turbulent flow, it is the correlation time and correlation length of the smallest eddies which are relevant here (that is, we identify τ and ξ with the Kolmogorov time and the Kolmogorov length of the turbulence, respectively).

The configuration of the rod can be specified by the position $\boldsymbol{r}(t)$ of its midpoint at time t and by a unit vector $\mathbf{n}(t)$ aligned with the rod (the binary ambiguity of the evolution is resolved by requiring continuity). The rods have an initial

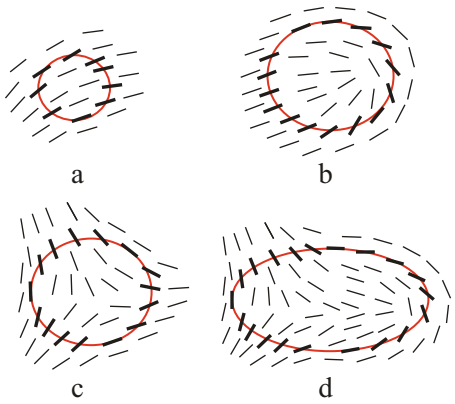

FIG. 4. (Color online) Given a nonoriented vector field $\mathbf{n}(\boldsymbol{r})$ in two dimensions and a closed curve $\mathcal{C}$, the Poincaré index $N(\mathcal{C})$ is defined as the number of multiples of 2π by which the direction of $\mathbf{n}$ rotates (in the clockwise direction) as $\mathcal{C}$ is traversed (also clockwise). For a nonoriented vector field, such as the direction of the rods, the Poincaré index may take half-integer values. (a) For a field without singularities, $N=0$. (b) For a curve which encircles a core, $N=\frac{1}{2}$. This singularity can be regarded as having a *charge* of $N=\frac{1}{2}$. (c) For a curve which encircles a delta, $N=-\frac{1}{2}$. (d) For a curve which encircles more than one singularity, their charges are summed. This curve encircles a combination of a core and delta which is termed a *loop*. For this case $N=-\frac{1}{2}+\frac{1}{2}=0$.

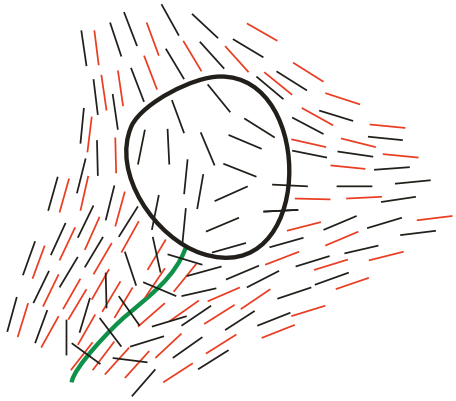

FIG. 5. (Color) The direction vector $\mathbf{n}$ (black lines) is asymptotic to the vector field of eigenvectors $\boldsymbol{u}_+$ (red lines). The vector field $\boldsymbol{u}_+$ is undefined in *gyres*, where the normal form of the monodromy matrix is a rotation. The Poincaré index of the field $\boldsymbol{u}_+$ on the boundary of the gyre need not be equal to zero, whereas the Poincaré index of $\mathbf{n}$ is zero. In these cases the field $\mathbf{n}$ rotates by π in the vicinity of one or more scar lines (green).

direction $\mathbf{n}_0$, which is a smooth function of the position $\boldsymbol{r}$. Our aim is to obtain equations of motion for $\boldsymbol{r}$ and $\mathbf{n}$, using these to understand the vector field $\mathbf{n}(\boldsymbol{r},t)$ describing the orientation of the rods which have reached position $\boldsymbol{r}$ at time t.

We simplify by assuming that the rod length a is very short compared to the correlation length ξ: $a/\xi \ll 1$. The center of the rod with position $\boldsymbol{r}$ is therefore assumed to move according to the advective equation of motion, $\dot{\boldsymbol{r}}=\boldsymbol{v}[\boldsymbol{r}(t),t]$ [we neglect small $O(a^2)$ corrections]. To obtain the equation of motion for the direction of the rod, we use a linear approximation for the velocity difference $\delta\boldsymbol{v}$ between the center of the rod, $\boldsymbol{r}$, and one of the particles at its ends, at $\boldsymbol{r}+\delta\boldsymbol{r}$,

$$\delta\boldsymbol{v}(\boldsymbol{r},t) = \mathbf{A}(\boldsymbol{r},t)\,\delta\boldsymbol{r}, \tag{2}$$

where $\mathbf{A}(\boldsymbol{r},t)$ is the strain-rate matrix (a 2×2 matrix with elements $A_{ij}=\partial v_i/\partial r_j$, which satisfies $\mathrm{tr}[\mathbf{A}]=0$ because $\boldsymbol{\nabla}\cdot\boldsymbol{v}=0$). The line between the two particles has direction specified by the unit vector $\mathbf{n}$. The equation for force balance on one of the particles at the end of the rod is $\dot{\boldsymbol{r}}=\boldsymbol{v}-T\mathbf{n}$, where $\boldsymbol{v}$ and $\dot{\boldsymbol{r}}$ are evaluated at the position of the particle at the end of the rod and where T is proportional to the tension in the rod, which keeps the separation of the two particles at its ends constant. Because $\dot{\boldsymbol{r}}=\boldsymbol{v}$ at the center of the rod, we obtain $\delta\dot{\boldsymbol{r}}=\delta\boldsymbol{v}-T\mathbf{n}$, and the equation of the constraint is $\delta\dot{\boldsymbol{r}}\cdot\mathbf{n}=0$. From these we find $T=\delta\boldsymbol{v}\cdot\mathbf{n}$. Combining these re-

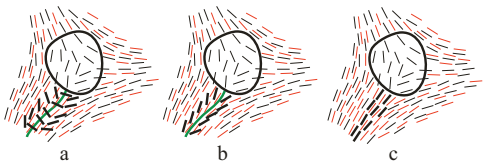

FIG. 6. (Color) (a) The rod direction (black) is a smooth vector field containing a scar line which ends on the boundary of a gyre. As time increases, the scar line narrows (b). When the scar line has narrowed to the extent that it does not include the actual position of any rod, it disappears (c). This leaves a point singularity at the end of the scar line: in this case a delta. In practice, the picture is more complex because the positions of the gyre and the scar line both change as time increases.

sults with Eq. (2) we find an equation of motion for $\mathbf{n}$,

$$\dot{\mathbf{n}} = \mathbf{A}\mathbf{n} - (\mathbf{n}\cdot\mathbf{A}\mathbf{n})\mathbf{n}. \tag{3}$$

This equation of motion is the same as that obtained by Jeffery[6] for a prolate ellipsoid of rotation, in the limit as the aspect ratio approaches infinity.

B. Solution of the equation of motion

We now consider how a solution of the equation of motion (3) may be obtained from the monodromy matrix of the flow. The solution which we describe below is a special case of one previously given in Ref. 7, but the very brief derivation is given below for completeness and in order to establish notations. The monodromy matrix $\mathbf{M}$ describes the evolution of the infinitesimal separation vector $\delta\boldsymbol{r}$ of two points advected by the flow, $\dot{\boldsymbol{r}}=\boldsymbol{v}(\boldsymbol{r},t)$: we write the separation of two points at time t in the form

$$\delta\boldsymbol{r}(t) = \mathbf{M}[\boldsymbol{r}(t),t,t_0]\delta\boldsymbol{r}(t_0). \tag{4}$$

Note that $\mathbf{M}$ is written as a function of the position $\boldsymbol{r}$ reached by the rod at time t and of the final and initial times t and t_0, respectively. The monodromy matrix satisfies the differential equation

$$\frac{d}{dt}\mathbf{M} = \mathbf{A}[\boldsymbol{r}(t),t]\mathbf{M}, \tag{5}$$

where $\boldsymbol{r}(t)$ is the trajectory of the center of the rod. The initial condition for Eq. (5) is $\mathbf{M}(\boldsymbol{r},t_0,t_0)=\mathbf{I}$, where $\mathbf{I}$ is the identity matrix for all positions $\boldsymbol{r}$. Now define $\mathbf{n}_0(\boldsymbol{r}_0)$ as the initial direction (at time t_0) of the rod, expressed as a function of the initial position $\boldsymbol{r}_0$. Let us consider the vector field

$$\mathbf{a}(t) = \mathbf{M}(\boldsymbol{r},t,t_0)\mathbf{n}_0(\boldsymbol{r}_0), \tag{6}$$

where $\boldsymbol{r}_0(\boldsymbol{r},t,t_0)$ is the initial position, at time t_0, of a rod which reaches $\boldsymbol{r}$ at time t. If we write $\mathbf{a}(t)=\alpha(t)\mathbf{n}(t)$, we find that $\mathbf{n}(t)$ satisfies the equation of motion (3) above. Also, it satisfies the initial conditions $\mathbf{n}(t_0)=\mathbf{n}_0[\boldsymbol{r}(t_0),t_0,t_0]$, since $\mathbf{M}(\boldsymbol{r},t_0,t_0)=\mathbf{I}$. Thus we can determine the orientation vector of the rods from the monodromy matrix by normalizing the vector $\mathbf{a}(t)$,

$$\mathbf{n}(\boldsymbol{r},t) = \frac{\mathbf{M}(\boldsymbol{r},t,t_0)\mathbf{n}_0(\boldsymbol{r}_0)}{|\mathbf{M}(\boldsymbol{r},t,t_0)\mathbf{n}_0(\boldsymbol{r}_0)|} \tag{7}$$

(where the initial position $\boldsymbol{r}_0$ is a function of $\boldsymbol{r}$, t, t_0).

C. Asymptotic form of the solution

Let λ_+ and $\boldsymbol{u}_+$ be, respectively, the eigenvalue of $\mathbf{M}$ with the largest magnitude and the corresponding eigenvector, normalized to unit length. We term these the dominant eigenvalue and eigenvector. The other eigenvalue and eigenvector are denoted λ_- and $\boldsymbol{u}_-$ and are termed subdominant. We assume that the random flow $\boldsymbol{v}(\boldsymbol{r},t)$ has a positive Lyapunov exponent, so that the elements of $\mathbf{M}(\boldsymbol{r},t,t_0)$ tend to increase exponentially as a function of $t-t_0$. (We remark that this assumption might not be valid in the case of simpler flows such as a recirculating flow.) Correspondingly $|\lambda_+/\lambda_-|$ is expected to increase exponentially (recall that $\lambda_+\lambda_-=1$). If $|\lambda_+/\lambda_-|\gg 1$, applying the matrix $\mathbf{M}$ to almost any vector is expected to result in a vector which is nearly aligned with $\boldsymbol{u}_+$. In particular, as $t-t_0\to\infty$ we expect that $\mathbf{n}(\boldsymbol{r},t)\sim\boldsymbol{u}_+(\boldsymbol{r},t)$ for almost all points in the plane. This is illustrated by the simulation in Fig. 7.

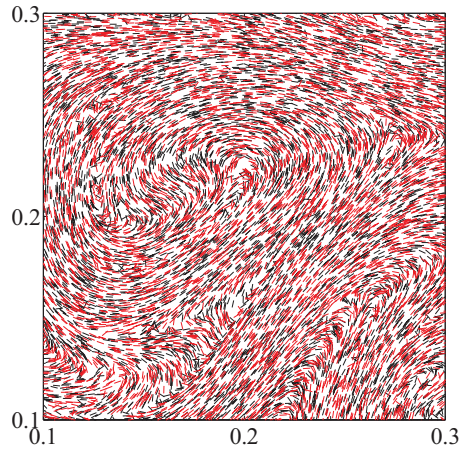

FIG. 7. (Color) Illustrating the correspondence between the rod direction field $\mathbf{n}(\boldsymbol{r},t)$ (black) and the eigenvector field $\boldsymbol{u}_+(\boldsymbol{r},t)$ (red) at large time.

III. APPARENT SINGULARITIES OF THE DIRECTION FIELD

Here we consider whether it is possible for the vector field $\mathbf{n}(\boldsymbol{r},t)$ to have singularities, where $\mathbf{n}$ changes discontinuously as a function of $\boldsymbol{r}$. First we show (Sec. III A) that it is not possible for $\mathbf{n}(\boldsymbol{r},t)$ to have singularities in a strict sense. It is, however, possible that the field could approach a singularity in some asymptotic sense. Accordingly, we also consider (Sec. III B) whether the eigenvector field $\boldsymbol{u}_+(\boldsymbol{r},t)$, to which $\mathbf{n}(\boldsymbol{r},t)$ is asymptotic, has any singularities. Although $\boldsymbol{u}_+(\boldsymbol{r},t)$ does not have singularities, we show that it can have a nontrivial topology. There are regions where the monodromy matrix $\mathbf{M}$ is elliptic (with conjugate eigenvalues on the unit circle) so that the dominant eigenvector $\boldsymbol{u}_+$ is not defined. We term these regions of rotational flow *gyres*. We find that the Poincaré index of the eigenvector $\boldsymbol{u}_+$ around the boundary of a gyre can be nonzero. In Secs. III C and III D we consider how the smooth field $\mathbf{n}(\boldsymbol{r},t)$ can be asymptotic to the topologically nontrivial field $\boldsymbol{u}_+(\boldsymbol{r},t)$.

A. Absence of singularities

For any finite value of $t-t_0$, the monodromy matrix $\mathbf{M}(\boldsymbol{r},t,t_0)$ is a smooth function of the final position of the trajectory, $\boldsymbol{r}$. The solution (7) can therefore only be discontinuous if the initial direction field is discontinuous or if the denominator $|\mathbf{M}\mathbf{n}_0|$ is equal to zero, which is only possible if there are points where $\det(\mathbf{M})=0$. This is not possible since we consider area-preserving flows, where $\det(\mathbf{M})=1$. If the initial direction vector field $\mathbf{n}_0(\boldsymbol{r})$ is nonsingular, we therefore conclude that the direction field $\mathbf{n}(\boldsymbol{r},t)$ remains nonsingular for all times. Because the vector field generated by Eq. (7) is smooth, the Poincaré index of this field is zero for any closed curve, in apparent contradiction to the simulations shown in Fig. 1.

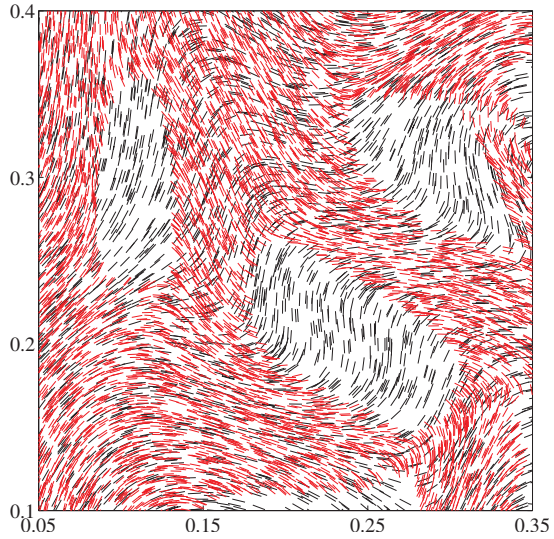

FIG. 8. (Color) Eigenvector field $\boldsymbol{u}_+(\boldsymbol{r},t)$ (red) and rod direction field $\mathbf{n}(\boldsymbol{r},t)$ (black) at small time $t-t_0$. The regions where there are no red vectors arise because the eigenvector field of the dominant eigenvalue of the monodromy matrix $\mathbf{M}(\boldsymbol{r},t,t_0)$ is undefined in regions (which we term gyres) where $\mathbf{M}(\boldsymbol{r},t,t_0)$ is elliptic. Note that at small $t-t_0$ the gyres occupy a large fraction of the area and have simple boundaries. In this figure it can be seen that two of the gyres have nonzero Poincaré index.

B. Topology of the eigenvector field

We have shown that the direction field $\mathbf{n}(\boldsymbol{r},t)$ is asymptotic to the field of eigenvectors, $\boldsymbol{u}_+(\boldsymbol{r},t)$. We shall see that the latter field has a nontrivial topology.

The only type of singularity of the eigenvector field which is possible is where the monodromy matrix is equal to the identity matrix. It is a codimension three condition for the monodromy matrix to have this form, so it is nongeneric in the two-dimensional problem which we consider. There is, however, another way in which the eigenvector field $\boldsymbol{u}_+(\boldsymbol{r},t)$ can have nontrivial topology.

In an area-preserving flow there will be regions of the plane where the eigenvalues are complex and have the same magnitude, so that $\boldsymbol{u}_+$ is undefined. We refer to these regions where the normal form of $\mathbf{M}(\boldsymbol{r},t)$ is a rotation as gyres. Each gyre is surrounded by a boundary. We find that the Poincaré index of the field $\boldsymbol{u}_+$ on the boundary of a gyre may not be equal to zero (two examples are illustrated in Fig. 8). This appears to contradict the result that $\mathbf{n}$ is asymptotic to $\boldsymbol{u}_+$ because we have seen that the Poincaré index of $\mathbf{n}$ is always zero.

C. Asymptotic singularities of the direction field

We have seen that $\mathbf{n}(\boldsymbol{r},t)$ is nonsingular, but that it is asymptotic to a vector field $\boldsymbol{u}_+(\boldsymbol{r},t)$ which may be topologically nontrivial. One way to resolve this contradiction is to assume that the field $\boldsymbol{u}_+(\boldsymbol{r},t)$ has become trivial by the time $\mathbf{n}(\boldsymbol{r},t)$ approaches it due to gyres with opposite topological charges coalescing. Our numerical studies show that this is not a sufficient explanation.

There is, however, another route to resolving this apparent contradiction which is both more interesting and which does lead to an explanation of the textures seen in Fig. 1. Let us consider the set of points where $\mathbf{n}$ need not be asymptotic to $\boldsymbol{u}_+$. There are two ways in which this can occur. Both lead to structures which we term scar lines.

We write the initial direction field as

$$\mathbf{n}_0 = \alpha_+ \boldsymbol{u}_+ + \alpha_- \boldsymbol{u}_-. \tag{8}$$

The vector $\mathbf{n}$ is proportional to $\mathbf{M}\,\mathbf{n}_0 = \alpha_+\lambda_+\boldsymbol{u}_+ + \alpha_-\lambda_-\boldsymbol{u}_-$. The assumption that the Lyapunov exponent γ is positive implies that at most positions the ratio of eigenvalues, $\lambda_+/\lambda_- \sim \exp(2\gamma|t-t_0|)$, grows exponentially as $t-t_0$ increases. We therefore expect that $\mathbf{n}$ aligns increasingly closely with $\boldsymbol{u}_+$. There are two ways in which this alignment can break down, leading to two types of scar lines.

1. Type I scar lines

The direction field $\mathbf{n}$ need not approach $\boldsymbol{u}_+$ when α_+ is sufficiently small. The locus where $\alpha_+=0$ forms a set of lines in the plane, and as we cross these lines the direction of $\mathbf{n}$ rotates by $\pm\pi$. We term these lines *type I scar lines*. The vector $\mathbf{n}$ differs significantly from $\boldsymbol{u}_+$ when $|\alpha_+|\exp(2\gamma|t-t_0|)=O(1)$. This region where the direction flips therefore becomes vanishingly small at $t-t_0\to\infty$. Accordingly, we can think of the scars lines as "healing over," that is, becoming invisible.

These scar lines must terminate at gyres. Figure 5 is a schematic illustration the fields $\mathbf{n}$ and $\boldsymbol{u}_+$ in the vicinity of a charged gyre and its associated scar line. Figure 9 shows type I scar lines in our numerical simulations.

2. Type II scar lines

Our argument that $\mathbf{n}$ aligns with $\boldsymbol{u}_+$ also fails if the eigenvalue ratio $|\lambda_+/\lambda_-|$ does not increase. The eigenvalue ratio is small in the vicinity of the gyres. The area of the gyres must decrease exponentially as $t-t_0$ increases. Generically, the gyres will be stretched and folded, as well as decreasing in area. In the long-time limit, the gyres occur in the form of very narrow strips where $|\mathrm{tr}(\mathbf{M})|\leq 2$. Upon crossing this strip, the sign of λ_+ changes, and correspondingly the vector $\mathbf{M}\,\mathbf{n}_0$ smoothly reverses direction. This implies that the direction of $\mathbf{n}$ reverses on crossing these narrow gyres: these are the type II scar lines.

D. Disappearance of scar lines and emergence of point singularities

As noted in Sec. III C above, the width of the region around a scar line where the fields $\mathbf{n}$ and $\boldsymbol{u}_+$ are significantly misaligned shrinks as $t-t_0\to\infty$. As this region shrinks, eventually there is a small probability that any rod actually lies in the region where these vectors are misaligned. In this case, for all practical purposes the scar line has disappeared. Consider a loop which encircles the end of a scar line. Initially the Poincaré index of $\mathbf{n}$ about this loop is zero. When the angle change of $\pm\pi$ associated with crossing the scar line disappears, the Poincaré index of the circuit becomes $N=\pm\frac{1}{2}$. The disappearance of the scar line is therefore associated with the emergence of a point singularity at the positions where the ends of this line were located. This is illus-

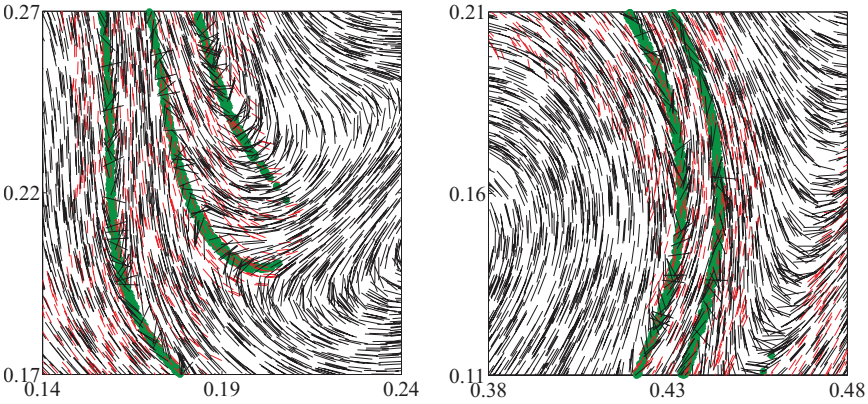

FIG. 9. (Color) Numerical examples of type I scar lines. The rod directions $\mathbf{n}$ are shown in black, eigenvector $\boldsymbol{u}_+$ is shown in red, and the position of the scar line is indicated by a sampling of points where $|\alpha_+|<10^{-2}$ (green). The direction of the rods is seen to flip around, rotating by approximately π, in the vicinity of the scar line.

trated schematically in Fig. 6, and by the numerical simulations in Fig. 10. This effect gives rise to the apparent singularities seen in Fig. 1.

E. A remark about eigenvector directions

We conclude this section by remarking that the eigenvectors $\boldsymbol{u}_+$ and $\boldsymbol{u}_-$ become colinear on the boundary of the gyre. This observation can be understood using the following argument. On the boundary of the gyre, the matrix $\mathbf{M}$ only has one eigenvalue (which may be +1 or −1). The set of 2 $\times 2$ matrices satisfying $\det \mathbf{M}=1$ has three parameters, and if the eigenvalues are constrained to be $\lambda=1$ (say), it becomes a two-parameter family of matrices. We now identify a parameterization of this family. Consider the eigenvalue equation, $\mathbf{F}\boldsymbol{u}=\lambda\boldsymbol{u}$, for matrices of the Jordan form,

$$\mathbf{F}(\kappa)=\begin{pmatrix}1 & \kappa\\ 0 & 1\end{pmatrix}. \tag{9}$$

These are a one-parameter family of matrices which have only one eigenvector, $\boldsymbol{u}=(1,0)$, and one eigenvalue, $\lambda=1$. If $\mathbf{R}$ is a rotation matrix

$$\mathbf{R}(\theta)=\begin{pmatrix}\cos\theta & \sin\theta\\ -\sin\theta & \cos\theta\end{pmatrix}, \tag{10}$$

we see that we can generate a two-parameter family of 2 $\times 2$ matrices $\mathbf{M}(\theta,\kappa)=\mathbf{R}^{-1}(\theta)\mathbf{F}(\kappa)\mathbf{R}(\theta)$ which have only one eigenvalue, $\lambda=1$. By construction of the matrix $\mathbf{M}(\theta,\kappa)$, we can show that this two-parameter family spans the set of 2 $\times 2$ matrices with only one eigenvalue, $\lambda=1$. But we have seen that these matrices have only one eigenvector, namely, $\boldsymbol{u}=\mathbf{R}(\theta)(1,0)^{\mathrm{T}}$. We conclude that as we approach the boundary of a gyre from the outside, the two eigenvectors $\boldsymbol{u}_+$ and $\boldsymbol{u}_-$ become colinear. This implies that α_+ and α_- both diverge as we approach the boundary of the gyre.

IV. THE LONG-TIME LIMIT

A. Sensitivity to final position

If we assume that the velocity field $\boldsymbol{v}(\boldsymbol{r},t)$ is statistically stationary, we expect that at long time the patterns formed by the rods also become statistically stationary (so that at long times it becomes impossible to estimate the time from the statistics of a realization of the rod positions). This property is, however, not manifest in the solution (7). As $t-t_0\to\infty$, the norm of the monodromy matrix grows. Also, while its elements are everywhere a smooth function of the initial position, the elements of $\mathbf{M}(\boldsymbol{r},t,t_0)$ do become ever more sensitive to the position $\boldsymbol{r}$ as $t-t_0\to\infty$. These observations suggest that as time increases the vector field $\mathbf{n}(\boldsymbol{r},t)$ should vary increasingly rapidly as a function of $\boldsymbol{r}$, the final position of the rods. We argue below that this is not the case, and that $\mathbf{n}(\boldsymbol{r},t)$ does reach a statistically stationary state.

If the eigenvector $\boldsymbol{u}_+(\boldsymbol{r},t)$ corresponding to the largest eigenvalue is less sensitive to the final position $\mathbf{r}$ than the matrix $\mathbf{M}(\boldsymbol{r},t,t_0)$ itself, then the apparent contradiction discussed above can be resolved. We now argue that this is, in fact, the case.

Let us consider a 2×2 random matrix $\mathbf{M}(t,t_0)$ generated

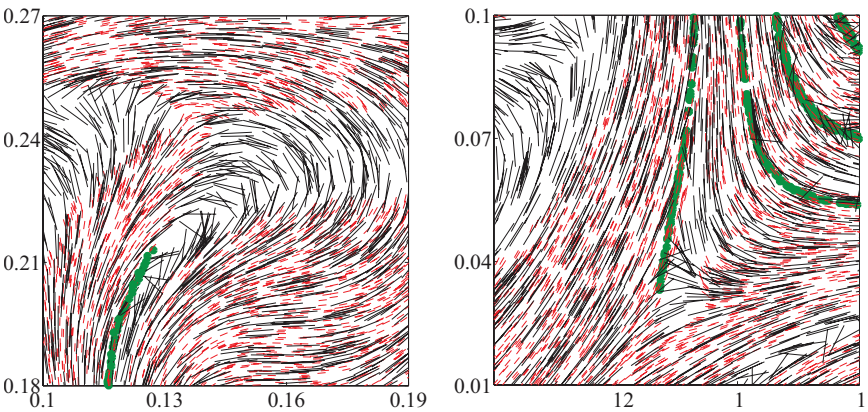

FIG. 10. (Color) Simulation showing healed scar lines. The rods are shown in black, and the eigenvector field is shown in red. The points in green show positions of rods where $|\alpha_+|<10^{-2}$ (and are therefore very close to scar lines). In these examples, because the scar line has become very narrow, the direction of the rods is not seen to flip around in the vicinity of the scar line, and the end of the scar line is marked by an apparent point singularity, namely, a loop (a) or a delta (b).

by an equation of motion $\dot{\mathbf{M}}=\mathbf{A}(t)\mathbf{M}$ [that is, by Eq. (5)], where $\mathbf{A}(t)$ is a traceless 2×2 matrix generated by a stationary random process. We apply the initial condition $\mathbf{M}(t_0,t_0)=\mathbf{I}$, where $\mathbf{I}$ is the unit matrix. The time dependence of the matrix $\mathbf{M}$ has a positive Lyapunov exponent γ describing exponential growth of the largest eigenvalue λ_+ as a function of $|t-t_0|$. Our discussion of the sensitivity of the solution will use an observation about the subdominat eigenvector $\boldsymbol{u}_-$, corresponding to the smallest eigenvalue λ_-. We start by showing that this eigenvector approaches a constant direction, which depends on the initial realization of $\mathbf{A}$ in the first few multiples of the Lyapunov time γ^{-1}. (The direction of the other eigenvector $\boldsymbol{u}_+$ continues to fluctuate randomly.)

To demonstrate this result, we consider the change in this eigenvector $\boldsymbol{u}_-(t)$ during a small timestep δt. Let $\mathbf{X}(t)$ be a matrix formed using the eigenvectors of $\mathbf{M}(t)$, such that $\mathbf{D}=\mathbf{X}\mathbf{M}\mathbf{X}^{-1}=\mathrm{diag}(\lambda+,\lambda_-)$ is the diagonal matrix formed from the eigenvalues of $\mathbf{M}(t)$. In the transformed basis, the matrix at time $t+\delta t$ is

$$\begin{aligned}\mathbf{M}' &= \mathbf{X}\mathbf{M}(t+\delta t)\mathbf{X}^{-1} = \mathbf{X}[\mathbf{I}+\mathbf{A}\,\delta t]\mathbf{M}\mathbf{X}^{-1} \\ &= [\mathbf{I}+\mathbf{A}'(t)\,\delta t]\mathbf{D}, \end{aligned} \tag{11}$$

where $\mathbf{A}'=\mathbf{X}\mathbf{A}\mathbf{X}^{-1}$. We write the eigenvalue equation for the subdominant eigenvalue of the matrix $\mathbf{M}$, with subdominant eigenvector $\boldsymbol{u}_-$,

$$\begin{aligned}\mathbf{M}'\boldsymbol{u}_- &= \begin{pmatrix} 1+A'_{11}\delta t & A'_{12}\delta t \\ A'_{21}\delta t & 1+A'_{22}\delta t \end{pmatrix}\begin{pmatrix} \lambda_+ & 0 \\ 0 & \lambda_- \end{pmatrix}\begin{pmatrix} \delta u'_- \\ 1 \end{pmatrix} \\ &= \begin{pmatrix} \lambda_+(1+A'_{11}\delta t) & \lambda_- A'_{12}\delta t \\ \lambda_+ A'_{21}\delta & \lambda_-(1+A'_{22}\delta t) \end{pmatrix}\begin{pmatrix} \delta u'_- \\ 1 \end{pmatrix} \\ &= (\lambda_- + \delta\lambda_-)\begin{pmatrix} \delta u'_- \\ 1 \end{pmatrix}. \end{aligned} \tag{12}$$

Neglecting terms of higher order in δt, the first element of this eigenvalue equation gives

$$\delta u'_- = -\frac{\lambda_-}{\lambda_+ - \lambda_-}A'_{12}\delta t. \tag{13}$$

In the limit as $t\to\infty$ the eigenvalues satisfy $|\lambda_+/\lambda_-|\to\infty$ and $\delta u'_-/\delta t\to 0$. We therefore conclude that the eigenvector of the subdominant eigenvalue approaches a constant direction. Writing the eigenvector of the dominant eigenvalue of $\mathbf{M}'$ as $\boldsymbol{u}_+=(1,\delta u'_+)$, the corresponding expression is

$$\delta u'_+ = A'_{21}\delta t. \tag{14}$$

Here the coefficient of δt does not approach zero as $t\to\infty$, and we conclude that the dominant eigenvector continues to rotate in the large time limit.

Now, given the orientations of the rods at time t, let us consider their orientations at the earlier time t_0. This map is determined by a time-reversed version of Eq. (3). Its solution is constructed by analogy with Eq. (7), replacing $\mathbf{M}$ with $\mathbf{M}^{-1}$. The eigenvector of $\mathbf{M}(t,t_0)$ corresponding to its largest eigenvalue is also the eigenvector of $\mathbf{M}^{-1}(t,t_0)$ corresponding to its smallest eigenvalue. Using the result discussed above, the eigenvector corresponding to the smallest eigenvalue of $\mathbf{M}^{-1}(t,t_0)$ becomes insensitive to t_0 when $\gamma|t-t_0|\gg 1$ (where γ is the Lyapunov exponent of the flow). Correspondingly, the eigenvector of $\mathbf{M}(t,t_0)$ corresponding to the largest eigenvalue becomes insensitive to t_0. We conclude that although the matrix $\mathbf{M}(t,t_0)$ has an increasingly sensitive dependence on position as $t-t_0\to\infty$, the eigenvector $\boldsymbol{u}_+$ does not become increasingly sensitive. Because the rod directions are asymptotic to these vectors, the rod directions do not become increasingly sensitive to the position $\boldsymbol{r}$ as time increases, except in the vicinity of gyres.

There are regions where the matrix $\mathbf{M}$ is not hyperbolic, so that there is no largest eigenvalue and consequently $\boldsymbol{u}_+$ is not defined. However, as $|t-t_0|\to\infty$, the norm of $\mathbf{M}$ increases almost everywhere, and the fraction of the area of the plane occupied by regions where $\boldsymbol{u}_+$ is not defined approaches zero.

We conclude that as $t-t_0\to\infty$, the vector field $\mathbf{n}(\boldsymbol{r},t)$ is statistically stationary, approaching the vector field $\boldsymbol{u}_+(\boldsymbol{r},t)$ almost everywhere.

B. Distribution of angle gradients

We have seen that the rod directions do not become increasingly sensitive to position as time increases. It is desirable to quantify the sensitivity to position. We have seen that the textures formed by the rod orientations show regions where the rod direction varies very rapidly with position, relative to other regions. Earlier, we described how the existence of scar lines explains the structures seen in specific realizations of the patterns. In this section we consider the probability distribution of the angle gradient, showing that the distribution is very broad, being well approximated by a log-normal distribution. This very broad distribution of the angle gradient is consistent with the existence of the structures described in Sec. III.

We now consider how to calculate the angle gradient $\boldsymbol{g}=\boldsymbol{\nabla}\theta$. In the following, we obtain an expression for one component, g_1, of $\boldsymbol{g}$. We obtain an equation for g_1, Eq. (18), which is easily argued to be log-normally distributed. It is, however, less clear that this formula for g_1 gives results which are well defined. We discuss this point in some detail after deriving Eq. (18), before finally presenting a brief argument that g_1 is approximately log-normally distributed at the end of this section.

Consider the difference between the eigenvector direction between two monodromy matrices evaluated along neighboring trajectories. The reference trajectory has monodromy matrix $\mathbf{M}(t)$ and the neighboring trajectory has monodromy matrix $\mathbf{M}(t)+\delta\mathbf{M}(t)$. We have seen that the subdominant eigenvector $\boldsymbol{u}_-$ of each monodromy matrix approaches a constant direction as $t\to\infty$, so the angle between them, $\delta\theta(t)$, must approach a constant value, that is, $\delta\theta(t)\to\delta\theta_\infty$ as $t\to\infty$. Let $\delta\mathbf{M}(t)$ be the change in the monodromy matrix due to shifting the end point of the trajectory at time t from $\boldsymbol{r}=(r_1,r_2)$ to $\boldsymbol{r}+\delta\boldsymbol{r}=(r_1,r_2)+(\delta r_1,0)$. The first component of $\boldsymbol{g}$ is $g_1=\lim_{\delta r_1\to 0}\delta\theta/\delta r_1$.

We introduce an orthonormal basis $\boldsymbol{u}_1$, $\boldsymbol{u}_2$ satisfying $\boldsymbol{u}_i\cdot\boldsymbol{u}_j=\delta_{ij}$, where $\boldsymbol{u}_2=\boldsymbol{u}_-(t)$ is the subdominant eigenvector of $\mathbf{M}(t)$. The elements of $\mathbf{M}$ in this basis are $M'_{ij}=\boldsymbol{u}_i\cdot\mathbf{M}(t)\boldsymbol{u}_j$, which form the matrix

$$\mathbf{M}' = \begin{pmatrix} M'_{11} & 0 \\ M'_{21} & \lambda_- \end{pmatrix}. \tag{15}$$

When the end point of the rod trajectory is shifted by a distance $\delta\boldsymbol{r}=(\delta r_1,0)$, the matrix $\mathbf{M}'$ is perturbed to $\mathbf{M}'+\delta\mathbf{M}'$, and the angle of the subdominant eigenvector $\boldsymbol{u}_-$ changes by a small amount $\delta\theta$, which can be obtained by solving the eigenvalue equation

$$\begin{pmatrix} M'_{11}+\delta M'_{11} & \delta M'_{12} \\ M'_{21}+\delta M'_{21} & \lambda_-+\delta M'_{22} \end{pmatrix}\begin{pmatrix} \delta\theta \\ 1 \end{pmatrix} = (\lambda_- + \delta\lambda_-)\begin{pmatrix} \delta\theta \\ 1 \end{pmatrix}. \tag{16}$$

Using the first line of this equation to solve for $\delta\theta$, retaining leading order terms we obtain

$$\delta\theta = -\frac{\delta M'_{12}}{M'_{11}-\lambda_-}. \tag{17}$$

Note that when t is large, so that $\lambda_+/\lambda_- \gg 1$, we may drop the term λ_- from the denominator and approximate the first element of the gradient vector by

$$g_1 = \lim_{\delta r_1\to 0}\frac{\delta\theta}{\delta r_1} \sim -\frac{\boldsymbol{u}_1\cdot\dfrac{\partial\mathbf{M}(t)}{\partial r_1}\boldsymbol{u}_2}{\boldsymbol{u}_1\cdot\mathbf{M}(t)\boldsymbol{u}_1}. \tag{18}$$

The angle gradient must approach a definite value as $t\to\infty$, but it is not immediately clear that this expression approaches a constant value. We must look at Eq. (18) more carefully to see why this is, in fact, true.

It is desirable to have an explicit expression for the coefficients $\delta M'_{ij}(t)$. Note that the monodromy matrix $\mathbf{M}(t)$ satisfying $d\mathbf{M}/dt=\mathbf{A}(t)\mathbf{M}$ can be approximated by a product

$$\mathbf{M}(t) = \lim_{\delta t\to 0}\prod_{j=1}^{\mathrm{Int}(t/\delta t)}[\mathbf{I}+\mathbf{A}(j\delta t)\delta t]. \tag{19}$$

Writing $\mathbf{B}=\partial\mathbf{A}/\partial r_1$, the monodromy matrix for the displaced trajectory is

$$\begin{aligned}\mathbf{M}(t)+\delta\mathbf{M}(t) &= \lim_{\delta t\to 0}\prod_{j=1}^{\mathrm{Int}(t/\delta t)}[\mathbf{I}+\mathbf{A}(j\delta t)\delta t+\mathbf{B}(j\delta t)\delta r_1\delta t] \\ &= \delta r_1\lim_{\delta t\to 0}\sum_{k=1}^{\mathrm{Int}(t/\delta t)}\prod_{j=1}^{\mathrm{Int}((t-t')/\delta t)} \\ &\quad\times[\mathbf{I}+\mathbf{A}(t'+j\delta t)\delta t]\mathbf{B}(k\delta t)\delta t\prod_{j=1}^{\mathrm{Int}(t'/\delta t)} \\ &\quad\times[\mathbf{I}+\mathbf{A}(j\delta t)\delta t]+O(B^2).\end{aligned} \tag{20}$$

We find

$$\frac{\partial\mathbf{M}(t)}{\partial r_1} = \int_0^t dt'\mathbf{M}(t,t')\mathbf{B}(t')\mathbf{M}(t',0). \tag{21}$$

Having obtained an expression for $\delta\mathbf{M}$, we return to considering why g_1, given by Eq. (18), is independent of t in the limit as $t\to\infty$. Let us introduce the initial time in the arguments of the monodromy matrix, writing the monodromy matrix giving displacements at time t in terms of those at time t_0 as $\mathbf{M}(t,t_0)$. Consider the vectors $\boldsymbol{v}_1=\mathbf{M}(t,0)\boldsymbol{u}_1$ and $\boldsymbol{v}_2=\delta\mathbf{M}(t,0)\boldsymbol{u}_2$, where $\boldsymbol{u}_1$, $\boldsymbol{u}_2$ are two arbitrary vectors. We will show that the vectors $\boldsymbol{v}_1,\boldsymbol{v}_2$ almost always become colinear as $t\to\infty$. First choose a time t_1 such that $(t-t_1)\gamma \gg 1$. Note that we can write $\mathbf{M}(t,t_0)=\mathbf{M}(t,t_1)\mathbf{M}(t_1,t_0)$. The direction of the vector $\boldsymbol{v}_1=\mathbf{M}(t,t_0)\boldsymbol{u}_1$ is almost always nearly colinear with the direction of the dominant eigenvector of $\mathbf{M}(t,t_1)$, independent of the vector $\boldsymbol{u}_1$. In the case of the vector $\boldsymbol{v}_2=\delta\mathbf{M}(t,t_0)\boldsymbol{u}_2$, note that we can write

$$\begin{aligned}\delta\mathbf{M}(t,t_0) &= \delta r_1\mathbf{M}(t,t_1)\int_{t_0}^{t_1}dt'\mathbf{M}(t_1,t')\mathbf{B}(t')\mathbf{M}(t',t_0) \\ &\quad+\delta r_1\int_{t_1}^{t}dt'\mathbf{M}(t,t')\mathbf{B}(t')\mathbf{M}(t',t_0) \\ &= \mathbf{M}(t,t_1)\delta\mathbf{M}(t_1,t_0)[1+O((t-t_1)/t)],\end{aligned} \tag{22}$$

so that to leading order $\boldsymbol{v}_2$ is also colinear with the dominant eigenvector of $\mathbf{M}(t,t_1)$. We conclude that the vectors $\boldsymbol{v}_1$ and $\boldsymbol{v}_2$ are almost always colinear, provided $\gamma(t-t_0)\gg 1$.

Let us consider the evaluation of Eq. (18) in the case where

$$\mathbf{M}=\mathbf{M}(t,t_0)=\mathbf{M}(t,t')\mathbf{M}(t',t_0)=\mathbf{M}_2\mathbf{M}_1, \tag{23}$$

where $\mathbf{M}_1=\mathbf{M}(t',t_0)$, $\mathbf{M}_2=\mathbf{M}(t,t',)$. Correspondingly, neglecting terms of order δr_1^2, we have

$$\delta\mathbf{M}=\mathbf{M}_2\delta\mathbf{M}_1+\delta\mathbf{M}_2\mathbf{M}_1. \tag{24}$$

We consider the case where $\gamma(t-t_0)\gg 1$, with $t>t'>t_0$. In order to establish that the angle $\delta\theta$ becomes asymptotically independent of time, we must show that $\delta\theta=\delta\theta_1$, where $\delta\theta$ is given by Eq. (18) and where $\delta\theta_1$ is the expression obtained by replacing $\delta\mathbf{M}$, $\mathbf{M}$ with $\delta\mathbf{M}_1$, $\mathbf{M}_1$. Thus [in view of Eq. (23) and (24)] we must demonstrate that

$$\delta\theta = -\frac{\boldsymbol{u}_1\cdot\delta\mathbf{M}_1\boldsymbol{u}_2}{\boldsymbol{u}_1\cdot\mathbf{M}_1\boldsymbol{u}_1} = -\frac{\boldsymbol{u}_1\cdot\mathbf{M}_2\delta\mathbf{M}_1\boldsymbol{u}_2}{\boldsymbol{u}_1\cdot\mathbf{M}_2\mathbf{M}_1\boldsymbol{u}_1} - \frac{\boldsymbol{u}_1\cdot\delta\mathbf{M}_2\mathbf{M}_1\boldsymbol{u}_2}{\boldsymbol{u}_1\cdot\mathbf{M}_2\mathbf{M}_1\boldsymbol{u}_1}. \tag{25}$$

The second term on the right-hand side of the equality is negligible because $\mathbf{M}_1\boldsymbol{u}_2=\lambda_-\boldsymbol{u}_-$ and $\lambda_-\to 0$ as $t\to\infty$. In the first term the additional factor of $\mathbf{M}_2$ makes no difference to the value of $\delta\theta$ only if the vectors $\delta\mathbf{M}_1\boldsymbol{u}_2$ and $\mathbf{M}_1\boldsymbol{u}_1$ are colinear. But we argued above that these vectors are asymptotically colinear in the limit as $\gamma(t-t_0)\to\infty$. Thus we conclude that the angle $\delta\theta$ between two subdominant eigenvectors $\boldsymbol{u}_-$ in forward-time propagation does become independent of time as $t\to\infty$, justifying Eq. (18). We can now use the arguments of Sec. IV A to draw conclusions about the dependence of the reverse-time propagation of the dominant eigenvectors $\boldsymbol{u}_+$, which determine the rod direction. In particular, we conclude that the angle gradient at time t does become independent of the initial time t_0 as $t-t_0\to\infty$.

We have seen that the angle gradient of the orientation field of the rods remains finite in the long-time limit. It is of interest to consider the probability distribution of the angle gradient. We shall argue that this quantity has an approximately log-normal distribution. We note that the monodromy

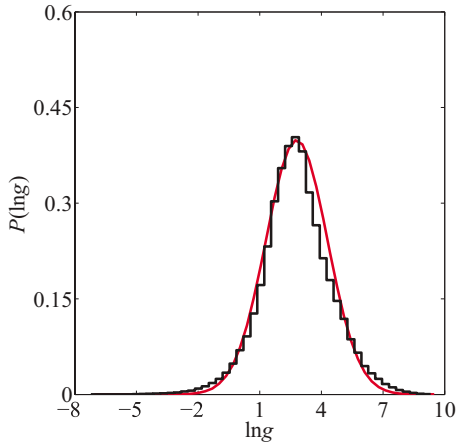

FIG. 11. (Color online) Histogram of the probability density of the angle gradient, showing that this has an approximately log-normal distribution. The parameter values of the simulation are the same as for the other figures.

matrix may be expressed as a product of a large number of independent random factors. It is clear that when $\gamma t \gg 1$, the distributions of the matrix elements of both $\delta\mathbf{M}$ and $\mathbf{M}$ are log normal. The distribution of their ratio is also log normal. We conclude that the distribution of the angle gradient, given by Eq. (18), is therefore also log normal at large times, provided the correlation time τ is short compared to the Lyapunov time γ^{-1}. In Fig. 11 this result is illustrated by a histogram of the distribution of the logarithm of the angle gradient for the same parameter values as used in the other numerical simulations. A Gaussian fit matches the histogram very closely.

V. DISCUSSION OF THE ROD TEXTURES IN THE LONG-TIME LIMIT

We have shown that the rod textures seen on Fig. 1 may be understood in terms of concepts introduced in Sec. III. We showed that the direction field $\mathbf{n}(\boldsymbol{r},t)$ is asymptotic to the vector field of the dominant eigenvector $\boldsymbol{u}_+(\boldsymbol{r},t)$ of the monodromy matrix $\mathbf{M}(\boldsymbol{r},t)$. However, we observed that $\mathbf{n}$ has a simple topology, whereas $\boldsymbol{u}_+$ has a nonzero Poincaré index upon traversing boundaries of some of its gyres. In order to reconcile the different topologies of these fields, we noted that this asymptotic correspondence breaks down on scar lines, where the direction vector $\mathbf{n}$ rotates abruptly by π. We showed that the size of the region where the direction reverses can decrease as the norm of the monodromy matrix increases, so that these scar lines can heal over when they become sufficiently narrow that it is unlikely that a rod lies in the region of the scar line. When the scar line has healed, there appears to be a point singularity with nontrivial topology at each of its ends.

In the long-time limit, the application of these concepts requires careful consideration. This is because, at very large times, the monodromy matrix $\mathbf{M}(\boldsymbol{r},t)$ becomes increasingly sensitive to the final position of the rods, $\boldsymbol{r}$. As $t-t_0$ increases the gyres may shrink in area, their boundaries may stretch, and they may merge together. Also, gyres with a zero Poincaré index may disappear. We expect that at very large times, the gyres are extended into lines where $\mathrm{tr}(\mathbf{M})$ changes sign. These lines are expected to become ever more closely spaced as $t-t_0 \to \infty$, with typical spacing $\xi \exp(-\lambda|t-t_0|)$. Following the reasoning presented in Sec. III, at large $t-t_0$, we expect that $\boldsymbol{u}_+$ fluctuates on a lengthscale ξ, independent of $t-t_0$. The definition of the type I scar lines depends on the initial direction field, and these structures are therefore expected to become irrelevant at very large times.

In order to discuss the long-time limit, we consider an expression for the direction field $\mathbf{n}(\boldsymbol{r},t)$ in terms of the dominant eigenvector field. Let $\mathbf{M}(\boldsymbol{r},t,t_0)$ be the monodromy matrix for a trajectory reaching $\boldsymbol{r}$ at time t, starting at time t_0, and let $\boldsymbol{u}_+(\boldsymbol{r},t,t_0)$ be the corresponding dominant eigenvector. As $t-t_0 \to \infty$ we expect that $\mathbf{n}(\boldsymbol{r},t) \sim \boldsymbol{u}_+(\boldsymbol{r},t)$ for almost all points in the plane. We can therefore construct the vector field $\mathbf{n}(\boldsymbol{r},t)$ from the dominant eigenvector $\boldsymbol{u}_+(\boldsymbol{r},t,t_0)$ as follows:

$$\mathbf{n}(\boldsymbol{r},t) = \lim_{t_0 \to -\infty} \boldsymbol{u}_+(\boldsymbol{r},t,t_0). \tag{26}$$

Let us consider the way in which this limit is approached, keeping t fixed and letting $t_0 \to -\infty$, starting from a time $t_0 = t - \delta t$ which is very close to t. We know that there exist gyres which shrink, stretch, and fold as $t_0 \to -\infty$, and that the Poincaré index of $\boldsymbol{u}_+$ about the boundary of these gyres may be nonzero. The observation that the field $\boldsymbol{u}_+(\boldsymbol{r},t_0,t)$ is topologically nontrivial begs the question as to how Eq. (26) can be correct, if $\mathbf{n}(\boldsymbol{r},t)$ has no singularities. There are two possibilities for the manner in which the limit $t-t_0 \to \infty$ is approached. The first possibility is that gyres with opposite topological charges combine, so that in the limit the field $\boldsymbol{u}_+(\boldsymbol{r},t,t_0)$ becomes topologically trivial. Numerical experiments indicate that this case is not realized in practice. The other possibility is that as the gyres shrink the field $\mathbf{n}(\boldsymbol{r},t)$ can develop singularities which shrink in size and which cause no abrupt changes in their direction except in the vicinity of the gyres. We have seen that there exist type II scar lines where the direction of $\mathbf{n}(\boldsymbol{r},t)$ changes by π on crossing a narrow gyre.

As $t_0 \to -\infty$, the gyres become narrower and the scar lines heal over, that is, there is unlikely to be any particle close to the gyre, so that the gyres therefore have no visible effect on the field $\mathbf{n}(\boldsymbol{r},t)$. Consider a loop which encircles the end of a type II scar line. Initially the Poincaré index of $\mathbf{n}(\boldsymbol{r},t)$ about this loop is zero. When the angle change of $\pm\pi$ associated with crossing, the scar line disappears as the scar line heals over, the Poincaré index of the circuit becomes $N = \pm\frac{1}{2}$. The disappearance of the scar line is therefore associated with the emergence of a point singularity at the positions where the ends of this line were located.

What can we say about the rod textures at long times? We have shown in this section that the patterns formed by the eigenvector field $\boldsymbol{u}_+(\boldsymbol{r},t,t_0)$ are statistically stationary for long times because the direction of the dominant eigenvector is determined only by the recent history of the monodromy matrix, over a few multiples of its Lyapunov time, γ^{-1}. This is true despite the fact that the elements of $\mathbf{M}(\boldsymbol{r},t,t_0)$ have unbounded growth and become increasingly sensitive to $\boldsymbol{r}$ as $t-t_0 \to \infty$. We have also presented an argument showing how

the direction field $\mathbf{n}(\boldsymbol{r},t)$ and its apparent singularities are obtained from the dominant eigenvector field using Eq. (26). We conclude that the textures of the direction field are also statistically stationary in the long-time limit.

VI. THREE-DIMENSIONAL FLOWS

Thus far, we have considered textures in two-dimensional flows. We conclude by considering what additional structures might arise when the flow is three dimensional. The principal difference is that in a three-dimensional flow the direction vector $\mathbf{n}(\boldsymbol{r},t)$ covers a sphere rather than a circle (it remains nonoriented), but the equation of motion (3) and its solution (7) have the same form. In three dimensions, there are many new questions which can be addressed, and some of the implications of the solution (7) for three-dimensional flows have been considered in Refs. 7 and 10. Here we confine ourselves to a discussion of those aspects which are relevant to the experiment discussed in Sec. I, where we showed how a rheoscopic fluid can be studied using illumination by colored lights. In the three-dimensional case, the interpretation of experimental results is most straightforward if the rheoscopic agent is sufficiently concentrated that the reflected light comes from the surface layer of the liquid (that is, if the optical depth is small compared to the characteristic scale of the flow). We confine our discussion to this case.

For the problem which we consider, the color of the scattered light is determined solely by the direction of the projection of $\mathbf{n}(\boldsymbol{r},t)$ in the plane of the fluid surface, evaluated at a point on the fluid surface. This projected vector field, $\mathbf{n}_p(\boldsymbol{r},t)$, can have singularities if there are positions where the rods point out of the surface of the liquid. The projected vector field $\mathbf{n}_p(\boldsymbol{r},t)$ then has a simple zero, which has Poincaré index +1, as well as the fingerprintlike singularities which we discuss above.

Our explanation for the occurrence of apparent singularities with Poincaré index $\pm\frac{1}{2}$ depends on the existence of gyres, where there is no dominant eigenvalue, and where the eigenvector has a nonzero Poincaré index on traversing the boundary. In the three-dimensional case, we must consider how these concepts are modified.

In three-dimensional volume preserving flow, the monodromy matrix satisfies $\det(\mathbf{M})=1$. Apart from degenerate cases the monodromy matrix $\mathbf{M}$ has three possible spectral types.

(1) Eigenvalues real and distinct, with at least one of them greater than unity. The axis of the particle aligns with the eigenvector $\boldsymbol{u}_+$ corresponding to the largest eigenvalue, λ_+.
(2) There may be a real eigenvalue $\lambda_+>1$ and a complex pair with modulus less than unity. In this case the axis also aligns with $\boldsymbol{u}_+$.
(3) There may be two complex-conjugate eigenvalues having modulus greater than unity, with complex-conjugate eigenvectors. When these two eigenvectors are combined with complex-conjugate coefficients, the resulting real vector lies in a plane.

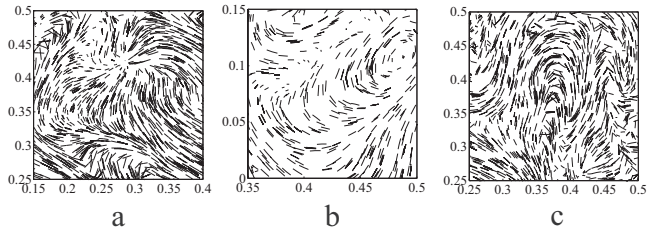

FIG. 12. Projected orientations of rods suspended in a three-dimensional flow. Only rods in a thin layer (with depth much smaller than the correlation length of the velocity field) are shown. These textures may have singularities due to the rods becoming perpendicular to the plane [(a) and (b)], as well as fingerprintlike singularities (c).

In three dimensions, we define the gyres as the regions where the spectrum is of type 3. These regions occupy a finite volume in a three-dimensional space. The arguments deployed in Sec. III are extended to the three-dimensional case by considering the projected vector $\mathbf{n}_p(\boldsymbol{r},t)$ in the plane of the fluid surface. This vector is asymptotic to the projection of the dominant eigenvector in the plane of the fluid surface, $\boldsymbol{u}_{+p}(\boldsymbol{r},t)$. The arguments of Sec. III remain valid provided the Poincaré index of $\boldsymbol{u}_{+p}(\boldsymbol{r},t)$ around the curve where the gyre intersects the fluid surface is nonzero for some of the gyres. Numerical experiments have shown that this condition is satisfied, so that on the surface of a three-dimensional flow the field $\mathbf{n}_p(\boldsymbol{r},t)$ does contain fingerprintlike textures, as well as simple singularities which have integer Poincaré index.

We remark that this observation has an interesting consequence for the three-dimensional structure of the gyres. If the plane is moved down through the fluid, the curve representing the intersection of the gyre with this plane will deform. If this curve shrinks to a point, by continuity the Poincaré index associated with $\boldsymbol{u}_{+p}(\boldsymbol{r},t)$ must be zero. A curve can be shrunk to a point on a surface with the topology of a sphere, but a surface with nonzero genus g can contain curves which cannot be shrunk to a point. It follows that the three-dimensional gyres include examples which are multiply connected (for example, a torus has $g=1$).

We conclude that if the flow is three dimensional, the fingerprint like textures still appear on the free surface, but that there are also points where the projected orientation vector field $\mathbf{n}_p(\boldsymbol{r},t)$ has simple zeros, with Poincaré index +1, due to rods aligning perpendicular to the surface. Figure 12 shows examples of the orientations of rodlike objects in a thin layer within a three-dimensional random flow, projected onto the plane of the paper. This figure shows the occurrence of singularities with Poincaré index +1 where the rods point out of the plane, as well as the continued existence of fingerprintlike textures in three-dimensional flows.

ACKNOWLEDGMENTS

The work of V.B. has been supported by a postgraduate studentship from the Open University. B.M. is supported by the Vetenskapsrådet and the Research Initiative "Nanoparticles in an interactive environment" at Göteborg University.

APPENDIX: MODEL VELOCITY FIELD

Our numerical simulations used a synthetic velocity field $\boldsymbol{v}(x,y,t)$ which was periodic in x, y (with period L) and in t (with period T), generated from a random stream function $\psi(x,y,t)$: the components of the velocity field are $v_x = \partial\psi/\partial y$, $v_y = -\partial\psi/\partial x$. The stream function is written in terms of its Fourier decomposition,

$$\psi(x,y,t) = \sum_{k_x}\sum_{k_y}\sum_{\omega} A(k_x,k_y,\omega)e^{\imath(k_x x + k_y y + \omega t)}, \tag{A1}$$

where k_x, k_y are integer multiples of $2\pi/L$ and where ω is an integer multiple of $2\pi/T$. The coefficients $A(k_x,k_y,\omega)$ are random Gaussian variables with the following properties:

$$\langle A(k_x,k_y,\omega)\rangle = 0,$$

$$\langle A(k_x,k_y,\omega)A^*(k_x',k_y',\omega')\rangle = \delta_{k_x k_x'}\delta_{k_y k_y'}\delta_{\omega\omega'}(v_0\xi)^2(2\pi)^{3/2}\frac{\xi^2\tau}{L^2 T} \times \exp\left(-\frac{k_x^2\xi^2 + k_y^2\xi^2 + \omega^2\tau^2}{2}\right),$$

$$A(k_x,k_y,\omega) = A^*(-k_x,-k_y,-\omega). \tag{A2}$$

In the limits where $L\to\infty$ and $T\to\infty$ where many Fourier coefficients contribute to the sums, the correlation function of $\psi(x,y,t)$ approaches a Gaussian form,

$$\langle \psi(x,y,t)\psi(x',y',t')\rangle = (v_0\xi)^2 \times \exp\left[-\frac{(x-x')^2 + (y-y')^2}{2\xi^2}\right]\exp\left[-\frac{(t-t')^2}{2\tau^2}\right]. \tag{A3}$$

The fast Fourier transform was used to calculate Fourier components at discrete time steps $t_n = n\delta t$. In the simulations we used $\tau = 0.1$, $\xi = 0.1$, $v_0 = 1.0$.

In all of the simulations the rods were all initially in the same direction, that is, $\mathbf{n}_0$ was independent of $\boldsymbol{r}$. The color mapping of Fig. 2 was produced using MATLAB.

[1] P. Matisse and M. Gorman, "Neutrally buoyant anisotropic particles for flow visualization," Phys. Fluids **27**, 759 (1984).
[2] Ö. Savaş, "On flow visualization using reflective flakes," J. Fluid Mech. **152**, 235 (1985).
[3] G. Gauthier, P. Gondoret, and M. Rabaud, "Motion of anisotropic particles: Application to visualisation of three-dimensional flows," Phys. Fluids **10**, 2147 (1998).
[4] S. T. Thoroddson and J. M. Bauer, "Qualitative flow visualization using colored lights and reflective flakes," Phys. Fluids **11**, 1702 (1999).
[5] E. R. Henry, *Classification and Uses of Finger Prints* (Routledge, London, 1900).
[6] G. B. Jeffery, "The motion of ellipsoidal particles immersed in a viscous fluid," Proc. R. Soc. London, Ser. A **102**, 161 (1922).
[7] A. J. Szeri, "Pattern formation in recirculating flows of suspensions of orientable particles," Philos. Trans. R. Soc. London, Ser. A **345**, 477 (1993).
[8] F. P. Bretherton, "The motion of rigid particles in a shear flow at low Reynolds number," J. Fluid Mech. **14**, 284 (1962).
[9] G. G. Lipscomb, M. M. Denn, D. U. Hur, and D. V. Boger, "The flow of fiber suspensions in complex geometries," J. Non-Newtonian Fluid Mech. **26**, 297 (1988).
[10] A. J. Szeri and L. G. Leal, "Orientation dynamics and stretching of particles in unsteady, three-dimensional fluid flows: unsteady attractors," Chaos, Solitons Fractals **4**, 913 (1994).
[11] R. Mallier and M. R. Maxey, "The settling of non-spherical particles in a cellular flow field," Phys. Fluids A **3**, 1481 (1991).
[12] A. J. Szeri, S. Wiggins, and L. G. Leal, "On the dynamics of suspended microstructure in unsteady, spatially inhomogeneous, two-dimensional fluid flows," J. Fluid Mech. **228**, 207 (1991).
[13] H. Shin and M. R. Maxey, "Chaotic sedimentation of spheroidal particles in a cellular flow field," Phys. Fluids A **3**, 1434 (1991).
[14] H. Shin and M. R. Maxey, "Chaotic motion of nonspherical particles settling in a cellular flow field," Phys. Rev. E **56**, 5431 (1997).
[15] P. G. de Gennes and J. Prost, *The Physics of Liquid Crystals* (Clarendon, Oxford, 1993).
[16] J. J. Feng, G. Sgalari, and L. G. Leal, "A theory for flowing nematic polymers with orientational distortion," J. Rheol. **44**, 1085 (2000).